Supplementary information

Enhancing near-infrared photocatalytic activity and upconversion luminescence of BiOCl: Yb^{3+}-Er^{3+} nanosheets with polypyrrole in-situ modification

Youzhun Fan, Tianhui Wang, Zhijie Wu, Qibing Li, Yingying Zhang, Zhaoyi Yin, Yongjin Li*, Jin Han, Qi Wang, Jianbei Qiu*, Zhengwen Yang and Zhiguo Song*

School of Materials Science and Engineering Kunming University of Science and Technology Kunming, 650093, PR China

*Corresponding Author.

E-mail: liyongjin@kust.edu.cn; songzg@kust.edu.cn; qiu@kust.edu.cn;

Table of contents

Section 1. Experiments

Materials

Er_2O_3 (4N), Yb_2O_3 (4N), $Bi(NO_3)_3·5H_2O$ (AR), 1-Butyl-3-methylimidazolium chloride (BMC) (97%), pyrrole (PY) (AR) were used as starting materials. $Er(NO_3)_3$ and $Yb(NO_3)_3$ were prepared by dissolving the corresponding rare earth oxide in HNO_3 under heating with agitation.

Synthesis

For the preparation of BiOCl:10%Yb^{3+}-1%Er^{3+} nanosheets with oxygen vacancies. Firstly, stoichiometric amounts of $Er(NO_3)_3$, $Yb(NO_3)_3$, $Bi(NO_3)_3·5H_2O$ and a certain amount of pyrrole monomer (PY) were added in 75 mL of distilled water and then continuous stirred for 30 min. Subsequently, 3 mL BMC solution (1 mol/L) were slowly added to the above reaction solution under continuous stirring. After another 10 min of agitation, the mixture was transferred into a Teflon-lined stainless-steel autoclave of 100 mL capacity, and the autoclave was then placed in an oven with a temperature of 140℃ for 24 h. Naturally cooled to room temperature, the precipitates were washed with absolute alcohol and deionized water for several times. The resulting products were dried at 60℃ for 12 h. The BiOCl:10%Yb^{3+},1%Er^{3+} samples absence of oxygen vacancies was synthesized by the same process but without adding PY. To improve the crystallinity of the sample, the final products were annealed at 350℃ for 2 h in a sealed crucible, which was placed into a muffle furnace.

Characterization

The crystal structures of the samples were characterized by X-ray diffraction (XRD) (Bruker D8 Advance diffractometer using Cu Kα(λ= 1.5406 Å) radiation). The morphologies of the samples were studied using scanning electron microscopy (SEM, Hitachi SU-8220) with an acceleration voltage of 25 kV accompanied with energy dispersive spectroscopy (EDS) to examine the chemical composition. Transmission electron microscopy (TEM) and high-resolution transmission electron microscopy (HRTEM) of the samples were conducted using a TecnaiG2 TF30 electron microscope. The EPR (electron paramagnetic resonance) spectra were recorded on a Bruker Electron ParaMagnetic Resonance (A300). The UV-Vis-NIR absorption spectra of samples were

obtained by a spectrophotometer (Hitachi UV-4100), using the $BaSO_4$ as the reflectance sample. The chemical states were investigated by Thermo Fisher Scientific X-ray photoelectron spectroscopy (XPS, monochromatic Al Kα radiation), and the XPS data was calibrated by C 1s spectrum (binding energy is 284.8 eV). Photoluminescence spectra and decay profiles were recorded using an Edinburgh Instruments FLS980 spectrometer equipped with a 980 nm diode laser. The surface photovoltages (SPV) spectroscopic measurement was carried out based on the lock-in amplifier. It is composed of a monochromatic light source which provided by the 500 W xenon lamp (CHFXM-500 W, Global Xenon Lamp Power) and a monochromator (Omni-5007, Zolix), a lock-in amplifier (SR830-DSP) with a light chopper (SR540), a photovoltage cell and a computer. All the measurements were performed at room temperature. In addition, photocurrent analysis was conducted using an Electrochemical Workstation (Bio-Logic SP-300) with a standard three-electrode system. All the measurements were performed at room temperature.

Photocatalytic activity experiment

Photocatalytic efficiency of samples for RhB decomposition was tested under Vis (λ>400 nm), NIR light (λ>800 nm) and full spectra light irradiation with a 500 W Xe lamp (CEL-LAX500, Beijing China Education Au-light Co., Ltd). In a typical process, 20 mg photocatalyst was added into RhB aqueous solution (40 mL, 10 mg/L) under magnetic stirring for 1h in the darkness to guarantee the adsorption desorption equilibrium. During the illumination process, 3.5 mL of suspension was taken out at given time intervals and centrifuged to remove the remaining photocatalyst. The residual organic contaminants concentration was measured using a Hitachi UV-4100 spectrophotometer.

Further, in order to detect the generated active species in the photocatalysis. In this work, we use EDTA-2Na, IPA, and L-Ascorbic acid are used as scavengers for trapping photogenerated holes (h^+), hydroxyl radicals ($^{\cdot}OH$), and superoxide radicals ($^{\cdot}O_2^-$), respectively.

Theoretical calculations

In the present work, the calculations are performed using the CASTEP module

within the plane-wave pseudopotential method, along with the generalized gradient approximation (GGA) exchange and correlation functional in the scheme of Perdew-Burke-Ernzerhof (PBE).[1, 2] The valence electronic configurations are the states of Bi 6s6p, O 2s2p and Cl 3d4s4p for the ground-state electronic structure calculations. In order to get a good convergence of the geometry optimization, the cutoff energy is set as 400eV after a series of tests. Ultrasoft pseudopotential is adopted in the reciprocal space, and 4x4x1 Monkhorst Pack mesh grid is sufficient to reach convergence for 1x1x2 supercell calculations. All the atoms of the pure BiOCl and oxygen vacancies with BiOCl are fully relaxed to their equilibrium positions with an energy convergence of $1x10^{-5}$ eV while the force applied on each atom is less than 0.01 eV/Å.

Section 2. XPS

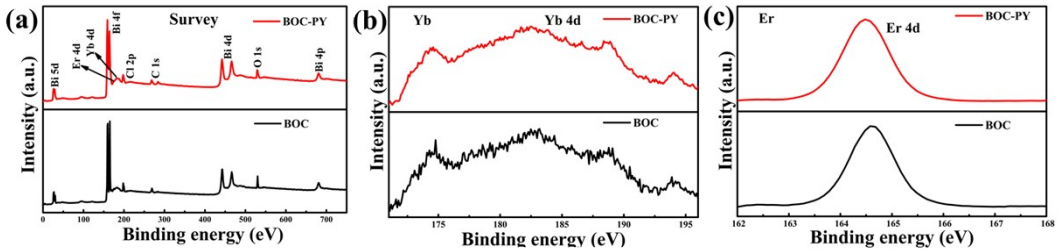

Fig. S1 XPS spectra of BOC and BOC-PY: (a) full survey spectrum, (b) Yb, (c) Er.

Section 3. the dielectric function

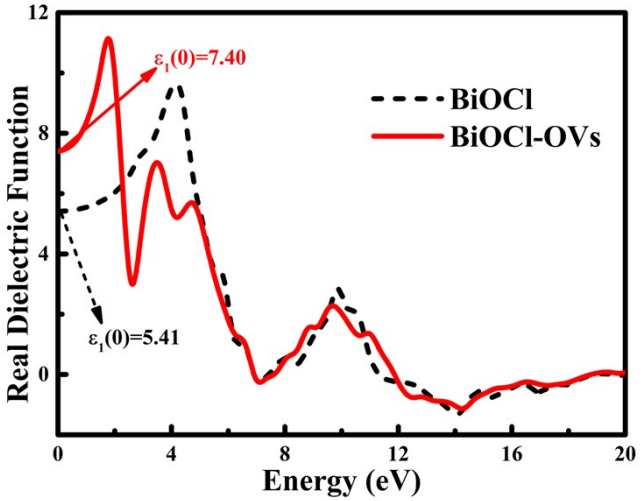

Fig.S2 Real part graph of the dielectric function of pure BiOCl and BiOCl-OVs.

To better prove the contribution of the electronic polarization of the OVs to the prepared samples, theoretical calculations of the optical properties were performed. This indicated that the OVs the polarization magnitude of BiOCl crystals greatly in the (001) direction. According to the theory of dielectric polarization and the depolarization intensity (P*d*) of the thin plate model:[3]

$$P_d = \frac{\chi \varepsilon_0}{1 + L\chi} E_{Ps} \quad (1)$$

$$\chi = \varepsilon_r - 1 \quad (2)$$

which P_d is the depolarization intensity, χ is the polarization coefficient, L is the depolarization factor (note: the depolarization factor of the thin plate model is 1), ε_0 and ε_r represent the permittivity of vacuum and relative dielectric constant, respectively, and E_{Ps} is spontaneous polarization electric field. The magnitude of E_{Ps} is proportional to the static dielectric constant $\varepsilon_1(0)$ values. Therefore, we can infer that the magnitude of the depolarization field and the IEF of BiOCl crystals in the (001) direction increase significantly by OVs engineering.

Section 4. Red-green ratio of PL spectrum

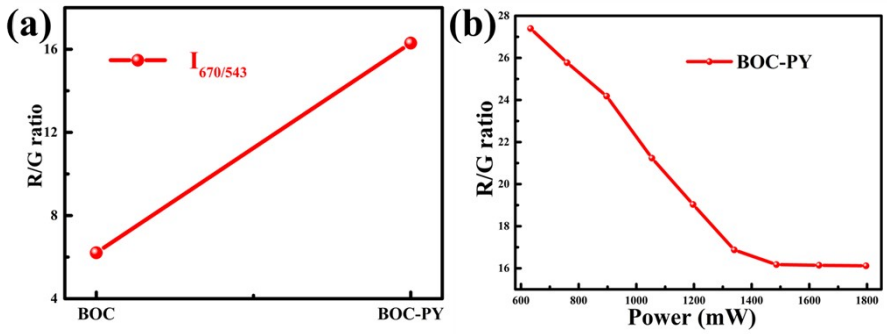

Fig. S3 (a) The calculated R/G ratio of the samples; (b) Relationship between red-green ratio and excitation power.

Section 5. The Photocatalytic activity

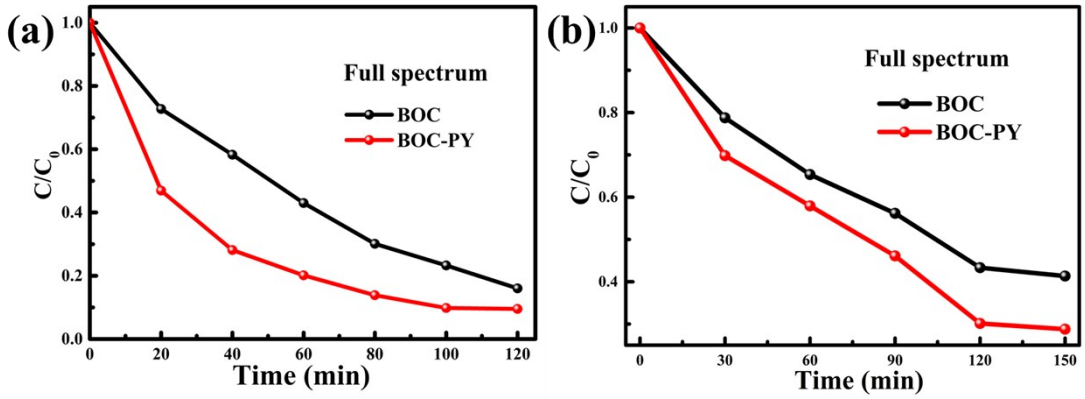

Fig. S4 The photocatalytic of BOC-PY and BOC-PY nanosheets (a) MB and (b) BPA.

Section 6. XPS-VB

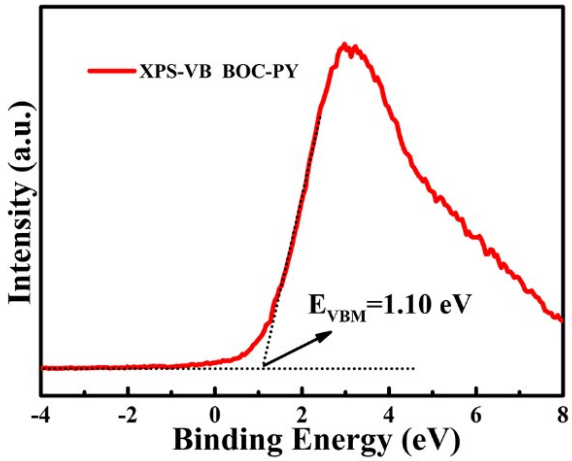

Fig. S5 The VB spectra of BOC-PY nanosheets.

Section 7. The photocatalytic mechanism of NIR irradiation.

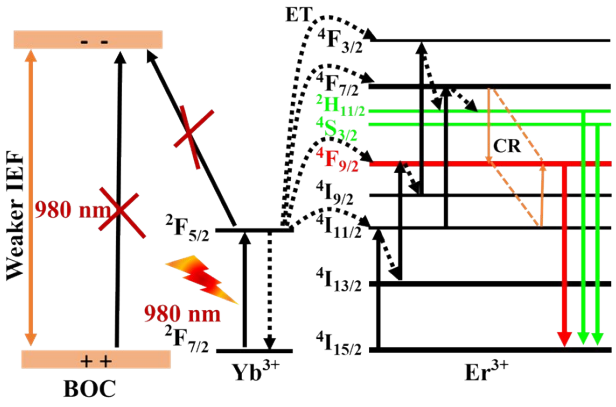

Fig. S6 The photocatalytic mechanism of BiOCl: Yb^{3+}-Er^{3+} nanosheet by NIR irradiation.

Section 8 Comparison of dye degradation

Table S1 Comparison of dye degradation between our material and similar reported materials in the literature

Photocatalyst	Light source power		Degradation rate			Ref.
	Vis (W)	NIR	Vis (min^{-1})	NIR (h^{-1})	Solar (min^{-1})	
BiOBr:Yb^{3+},Er^{3+}/ g-C_3N_4	1000 W	250 W	0.0264	0.3649	0.0523	4
$BiPO_4$:Yb^{3+}, Tm^{3+}/$BiVO_4$	140 W	980 nm	0.0107	0.0415	0.0471	5
$BiVO_4$/CaF_2: Er^{3+}, Tm^{3+}, Yb^{3+}	–	980 nm	–	0.0113	0.036	6
BiOBr:10%Yb^{3+}/ 1%Er^{3+}-OVs	500 W	500 W	0.0025	0.0258	0.0067	7
BiO_{2-x}/$Bi_2O_{2.75}$	500 W	500 W	0.0654	0.0094	0.1584	8
BOC-PY	500 W	500 W	0.0358	0.0334	0.0723	This work

References

1. S. J. Clark, M. D. Segall, C. J. Pickard, P. J. Hasnip, M. I. J. Probert, K. Refson and M. C. Payne, *Zeitschrift für Kristallographie-Crystalline Materials*, 2005, **220**, 567-570.
2. J. P. Perdew, A. Ruzsinszky, G. I. Csonka, O. A. Vydrov, G. E. Scuseria, L. A. Constantin, X. Zhou and K. J. P. r. l. Burke, 2008, **100**, 136406.
3. J. G. Kirkwood, *The Journal of Chemical Physics*, 1939, **7**, 911-919.
4. S. Liang, M. He, J. Guo, J. Yue, X. Pu, B. Ge and W. Li, *Separation and Purification Technology*, 2018, **206**, 69-79.
5. S. Ganguli, C. Hazra, M. Chatti, T. Samanta and V. Mahalingam, *Langmuir*, 2016, **32**, 247-253.

6. S. Huang, N. Zhu, Z. Lou, L. Gu, C. Miao, H. Yuan and A. Shan, *Nanoscale*, 2014, **6**, 1362-1368.
7. Y. Li, T. Liu, Z. Cheng, Y. Peng, S. Yang and Y. Zhang, *Chemical Engineering Journal*, 2021, **421**.
8. M. Wang, G. Tan, D. Zhang, B. Li, L. Lv, Y. Wang, H. Ren, X. Zhang, A. Xia and Y. Liu, *Applied Catalysis B: Environmental*, 2019, **254**, 98-112.